NJC

Accepted Manuscript

This article can be cited before page numbers have been issued, to do this please use: M. A. Betiha, N. G. Kandile, A. M. Badawi, S. Solyman and A. S. afify, *New J. Chem.*, 2018, DOI: 10.1039/C7NJ04007E.


Volume 40 | Number 1 | January 2016 | Pages 1–846
NJC
New Journal of Chemistry
www.rsc.org/njc
A journal for new directions in chemistry
ISSN 1144-0546
ROYAL SOCIETY OF CHEMISTRY
PAPER
Jaison B. Benedict et al.
The role of atropisomers on the photo-reactivity and fatigue of diarylethene-based metal–organic frameworks

ROYAL SOCIETY OF CHEMISTRY

rsc.li/njc

View Article Online
DOI: 10.1039/C7NJ04007E

p-Toluic Acid Oxidation to Terephthalic Acid via Bromine-Free Process Using Nano Manganese and Manganese-Copper Mixed Oxides

Mohamed A. Betiha[a,b], Nadia G. kandile[c], A. M. Badawi[b], Sanaa M. Solyman[b,d], and Ahmed S. Afify[b]

[a] *Egypt nanotechnology center (EGNC) Cairo university, El-Shiekh Zayed, 12588, Egypt.*

[b] *Egyptian Petroleum Research Institute, Nasr City, Cairo 11727, Egypt.*

[c] *Faculty of women for Arts, Science and Education, Ain Shams University, Cairo, Egypt*

[d] *AL-Ghad International College for Applied Medical Science, Kingdom of Saudi Arabia.*

The corresponding authors:

Ahmed S. Afify : ahmedsamyas@hotmail.com

Mohamed A. Betiha : mohamed_betiha@hotmail.com

DOI: 10.1039/C7NJ04007E

Abstract

The industrial process of terephthalic acid (TPA) production suffers from many environmental and economical drawbacks. Liquid phase catalytic oxidation of alkylbenzene by oxygen usually is initiated by bromine in a corrosive acetic acid solvent. A recent catalytic system used environmentally benign n-hydroxysuccinimide (NHSI) as a free radical promoter rather than more hazardous bromine molecules. Manganese dioxide and Cu-Mn mixed oxide nanoparticles with different ratios (CuMn11, CuMn12, and CuMn13) were prepared and examined as oxidation catalysts for p-toluic acid (p-TA) to produce TPA in an oxygen atmosphere. These catalyst samples were characterized by HRTEM, XRD, and N_2-adsorption-desorption isotherm techniques. The catalytic activity of prepared nanocatalysts for TPA was studied at different conditions (reaction time, catalyst dosages, reaction solvent and varied oxygen pressure and reaction temperature) to maximize the yield (%) and selectivity (%) toward TPA synthesis. Catalyst characterization indicates that CuMn11 sample has a new phase of the spinal structure. Furthermore, it is the most active catalyst that produces 99.5 and 99.6% in acetonitrile and ethylacetate solvents respectively under oxygen pressure 20 atm. and 150 °C.

Keywords:

Mixed metal oxides; Liquid phase oxidation; terephthalic acid (TPA)

View Article Online
DOI: 10.1039/C7NJ04007E

Introduction

Catalytic oxidation of methylbenzenes to corresponding alcohols, aldehydes and carboxylic acids by molecular oxygen is an important technique to fabricate useful oxygenated products [1-3]. For example, selective catalytic oxidation of p-xylene (PX) is a major industrial process for the production of TPA, which is an essential monomer for strong fabric polyesters production [4]. The commercial production of TPA is based on the liquid phase catalytic oxidation of PX by air or oxygen in the presence of ($Co(OAc)_2.4H_2O$), ($Mn(OAc)_2.4H_2O$) as homogeneous catalyst and Br_2 or HBr as a promoter in acetic acid as a solvent at temperature regime of 190–205 °C, pressures of 15 - 30 atm and reaction time of 8–24 h, acquiring a conversion of 95% and a selectivity of 90% [5]. However, acetic acid and Br_2 cause severe corrosions in equipment when used especially at high temperatures and give different unwanted by-products that complexed the separation process. Also, diluted acetic acid resulted from the catalytic process requires additional recovery and recycling units, and large amounts of acetic acid suffer from combustion in real plants to carbon oxides [6, 7]. Furthermore, Br_2 is very harmful to the human being, and cause serious environmental pollution.

The most promising promoters, N-hydroxyimides family as N-hydroxyphthalimide (NHPI), when mixed with transition metal salts in aerobic oxidation of organic compounds showed good activity reported by Ishii and coworkers [8-11]. Using this promoter in a catalytic process such as oxidation of alkylbenzenes by oxygen is a very important reaction for the production of bulk and fine chemicals such as benzoic acid and TPA [12]. Practically, the oxidation of toluene was carried out under normal oxygen pressure at room temperature by the use of a NHPI as promoter and Co(II) species as catalyst for the oxidation of PX to yield 85% p-TA (not TPA) after 20 h at room temperature by Ishii et al [9-11, 13-15] according to **(Scheme 1)**.

View Article Online
DOI: 10.1039/C7NJ04007E

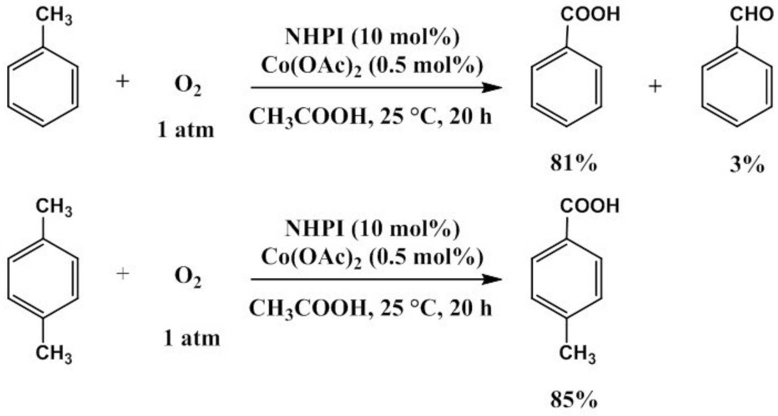

Scheme 1: Oxidation of alkylbenzenes with NHPI by oxygen

Various studies were reported including different transition metal ions like (Co(II), Mn(II), V(III) and Ce(IV), etc.) as homogeneous catalysts [16-20]. For example, the oxidation of PX with oxygen gas (1 atm) in presence of NHPI (20 mol%) and $Co(OAc)_2$ (0.5 mol%) as catalysts in acetic acid as solvent at 100 °C for 14 h to produced TPA in 67% yield and PTA (15%) associated with small amounts of (4-carboxybenzyl alcohol), 1,4-diacetoxymethylbenzene and 4-acetoxymethylbenzoic acid as well as several unidentified compounds in 1–2% yields, at over 99% conversion [21, 22]. The yield of TPA is improved to 82% when $Mn(OAc)_2$ (0.5 mol%) is added to the NHPI/$Co(OAc)_2$ system. The synergistic effect of Co and Mn salts in the aerobic oxidation of alkylbenzenes has been well documented [23-25]. The current situation is that the aerobic oxidation of PX is performed under air (30 atm) by the NHPI/Co/Mn system within 3 h at 150 °C to form TPA in 84% yield [26, 27] **(Scheme 2)**.

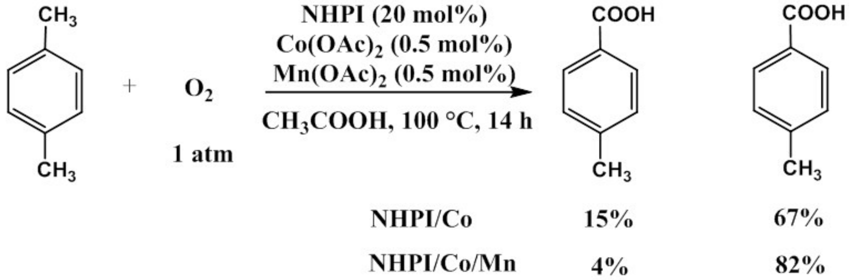

Scheme 2: Oxidation of PX by O_2 with NHPI/$Mn(OAc)_2$/$Co(OAc)_2$

This method has some advantages such as the use of environmentally benign, N-hydroxysuccinimide (NHSI), as a free radical promoter rather than a more hazardous

View Article Online
DOI: 10.1039/C7NJ04007E

bromine compound, coupled with the use of cheap and available oxidizing agent, oxygen gas, but keeps many disadvantages such as the difficulty of catalyst recovery and corrosion problems due to the presence of acetic acid. From an economic point of view, the use of nano transition metal oxides as heterogeneous catalysts that has considerable surface area rather than the soluble transition metals salts to overcome separation and recycling problems with a more environmentally friendly approach is one of the future solutions to this problem [28]**.**

Bulk and supported mixed metal oxides are extensively used in industry as heterogeneous oxidation catalysts [4]. These catalysts distinguished by variable oxidation states with redox properties, the contribution of a surface lattice oxygen atom and oxygen vacancies or defect sites in oxidation reactions [29]. Sabina Nicolae et al. [30] prepared mixed manganese iron oxides as heterogeneous catalysts by hydrothermal treatment and citrate methods to be studied in the oxidation of PX using different oxidizing agents. The results were negligible with molecular oxygen while conversion of PX of 98% and yield only in p-TA of 93% (not TPA) were obtained using *tert*-butyl hydroperoxide. At present, the AMCO process produced terephthalic acid using a homogeneous system of cobalt and manganese in the presence of dilute acetic acid [31]. Despite the high efficiency of cobalt and manganese catalyst used in Amoco [32], some alternative green technologies based on the use of carbon dioxide [33], water as a solvents [34], the use of heterogeneous catalysts such as Pd/ zeolite-Y [35] that enable recyclability are still need more development to meet the economic need for terephthalic acid production.

Herein, Cu-Mn mixed metal oxide, which is commercially available, is prepared with different ratios using co-precipitation technique and compared with single MnO_2-nanorods as liquid-phase oxidation catalysts in the presence of NHSI as promoter to oxidize p-TA, the main intermediate of TPA production [36] , which is more difficult stage of terephthalic acid production and formed with high yield rather than TPA [25, 37-39],with molecular oxygen and trying to replace the corrosive acetic acid with other solvents such as acetonitrile or ethylacetate, taking into account the environmental precautions of this process. Also, a detailed study was conducted to identify the degree of stability of the prepared catalysts. Various reactivity indexes have been analyzed including metal ratio, reaction time, catalyst dosages, pressure, and temperature in the

DOI: 10.1039/C7NJ04007E

presence of different solvents to provide an industrially applicable catalyst for the production of terephthalic acid.

2. Experimental

2.1. Materials

All chemicals and solvents were purchased and used without any further purification. p-toluic acid (p-TA), n-hydroxysuccinimide (NHSI), cobalt (II) acetate ($Co(OAc)_2.4H_2O$), manganese(II) acetate ($Mn(OAc)_2.4H_2O$), potassium permanganate ($KMnO_4$) were purchased from Sigma-Aldrich. All solvents like acetonitrile, glacial acetic acid, and ethyl acetate were obtained from Merck Chemical Co. The chloride salts of copper and manganese and sodium hydroxide were from El Nasr Chemical Co., Cairo, Egypt.

2.2. Preparation of nanocatalysts

2.2.1. Manganese dioxide (MnO_2) nanorods

$KMnO_4$ (6.5 gm) was charged into 150-ml round flask pre-charged with 150 ml water/ethanol (1:1). After complete dissolution, the flask is transferred to ultrasonic bath operated at 35 kHZ for 3 h. After that, 1 ml of H_2O_2 (30%) was added to complete the precipitation. The black precipitate of manganese oxide was collected by filtration and washed several times thoroughly with water to remove any residual of K^+ ions. The solid product was vacuum dried overnight at 60°C and was calcined at 400 °C for 2 h [40].

2.2.2. Copper- manganese mixed metal oxides

They were prepared using a coprecipitation method [41]. Aqueous solutions of $CuCl_2$ with definite concentration (0.2 mol/l) was mixed vigorously with different concentrations of xMnCl$_2$.6H$_2$O (where x = 0.2, 0.4, 0.6 mol/l) at 80 °C. Aqueous sodium hydroxide solution (NaOH) (0.25 mol/l) was added to the mixed solution slowly, drop by drop, with vigorous stirring while the temperature was maintained at 80 °C until pH = 9 was achieved. This procedure took approximately 2 h and the temperature continued at 80°C for further 3 h. The solution was then allowed to cool down to room temperature. The precipitate was then filtered, washed several times with warm distilled water for removal of Na^+ ions. The precipitate was then dried at 120 °C overnight and then was calcined at 300 °C in air for 4 h, giving the final catalysts which

View Article Online
DOI: 10.1039/C7NJ04007E

are dark black colored. They donated as CuMn11, CuMn12, and CuMn13 where the digits represented the molar ratios of Cu to Mn.

2.3. Characterization

Wide-angle X-ray diffraction pattern was recorded on an XPERT X-ray diffractometer in the angular range from 10 to 70 (2θ). The BET surface area, average pore diameter, and pore volume were measured at -196 °C on a NOVA 3200 system (USA). The catalysts were outgassed for 3 h at 300 °C under vacuum in the degassing port of the adsorption analyzer. The specific surface area was calculated using the BET model. The pore size distributions were obtained from the desorption branch of the nitrogen isotherms using Barrett-Joyner-Halenda (BJH) method. High-resolution transmission electron microscope (HRTEM) images were obtained using a JEOL JEM-2100 (Japan) operating at 200 kV. The X-ray photoelectron spectra were obtained using an ESCALAB MK II spectrometer provided with a hemispherical electron analyzer and Al anode X-ray exciting source (Al Kα =1487.6 eV).

All the oxidation reaction components (reactants, intermediates, promoter and products) were analyzed by using an HPLC (Waters model 2489) consists of an isocratic pump conducted through XBridge C18 column with an internal diameter of 4.6 mm, a length of 250 mm and a particle size of 5 µm equipped with ultraviolet detection (254 nm). The mixture of water/acetonitrile has a flow rate of 1mL/min with the injected volume of 20 µl was used in the isocratic mode at ambient temperature. Each sample analysis took about 12 min

2.4. Catalytic test

The catalytic activity was screened at refluxing and 1 atm, and then the catalytic reaction with the optimum conditions is carried out at different pressures and temperatures.

2.4.1. Catalytic oxidation of p-TA at atmospheric pressure

The oxidation of p-TA was performed in a 3-neck flask equipped with a magnetic stirrer and a septum for withdrawing samples at intervals of 1 h. The system was also equipped with a condenser to ensure complete condensation and recycling of the evaporated compounds. In a typical run, 80 mmol of p-TA, 16 mmol of NHSI, 0.4 mmol of $Co(OAc)_2$, 0.4 mmol of $Mn(OAc)_2$ and 250 ml of selected solvent

View Article Online
DOI: 10.1039/C7NJ04007E

(acetonitrile, ethylacetate or mixture of acetonitrile and acetic acid 9:1) were mixed in a glass batch flask. An appropriate weight of selected MnO_2 or Cu-Mn mixed oxide catalysts was added, and the stirring speed was set at 600 rpm. When the mixture was refluxed, pure oxygen was continuously bubbled into the solution mixture.

2.4.2. Catalytic oxidation of p-TA at high pressure (autoclave)

The high-pressure reactor is a 450 ml inconel autoclave. The system is also equipped with a condenser, a gas-liquid separator and a liquid recycle tank to ensure complete condensation and recycling of the evaporated compounds. The liquid-phase is continuously stirred at 193 rpm. The reactor temperature is regulated by an electric heating jacket with a thermocouple within ±0.2 °C, and a regulating valve controlled the reactor pressure.

The reactor was charged with the same concentrations of previous constituents (p-TA, NHSI, $Co(OAc)_2$, $Mn(OAc)_2$), selected solvent and catalyst weight from the best results obtained at 1 atm. After purging with pure oxygen, the reactor was closed during heating and agitated to attain the required pressure and temperature.

In atmospheric and pressurized reaction, the solid and mother liquor were separated by filtration. The clear liquid containing organic substrate, intermediates, and products were analyzed using an HPLC with an Ultraviolet detector with a suitable analytical method to calculate the yield, conversion, and selectivity percents for all compounds **Fig. 1.**

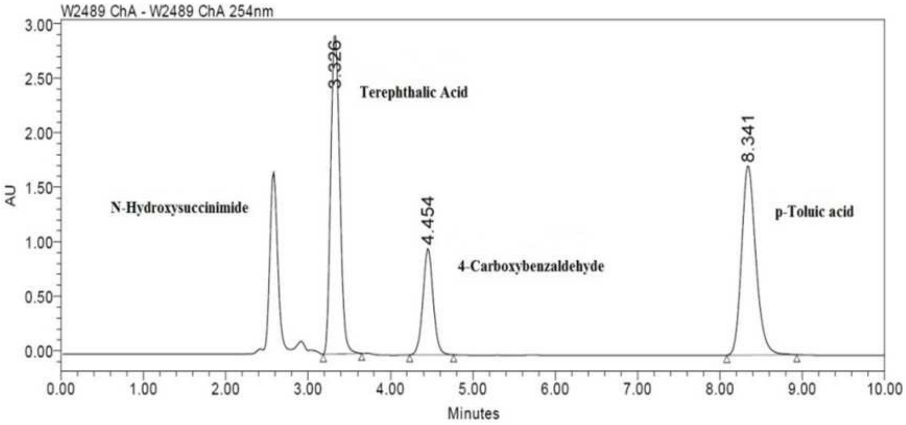

Fig. 1: HPLC chromatogram of all reaction components with retention time.

View Article Online
DOI: 10.1039/C7NJ04007E

3. Results and Discussion

In this work, the liquid-phase oxidation of p-TA was carried out under mild reaction conditions (about ≈87 °C and atmospheric pressure) at fixed concentrations of P-TA and NHSI as a promoter in presence heterogeneous catalysts as a recyclable catalyst. The discussion concentrates on the approach of green chemistry including (1) utilization of heterogeneous nanocatalysts with a different style, (2) study the effect of NHSI (instead of Br_2) as a promoter, and (3) replacement of corrosive acetic acid solvent by acetonitrile or ethyl acetate solvents.

3.1. Textural and Structural Characterization of different Mn/Cu-Mn oxides

3.1.1. X-ray diffraction analysis (XRD)

The crystalline phases of prepared catalysts were studied by X-ray diffraction analysis. As shown in **Fig. 2**, The XRD pattern of MnO_2 confirms the formation of its exact phase. The characteristic peaks at 12.5°, 18.07°, 28.65°, 37.3°, 41.95°, 49.85°, 59.74° and 65.15°, are well matched with the diffraction peaks (1 1 0), (2 0 0), (3 1 0), (2 1 1), (3 0 1), (4 1 1), (6 0 0) and (5 2 1) reflection planes of MnO_2 (JCPDS card PDF # 00-044-0141). The lattice parameters of caddice-clew-like MnO_2 are a = 9.7875 and c = 2.8600, are highly identical to the standard values (JCPDS card PDF file no. 44-0141, a = 9.7847, c = 2.863).

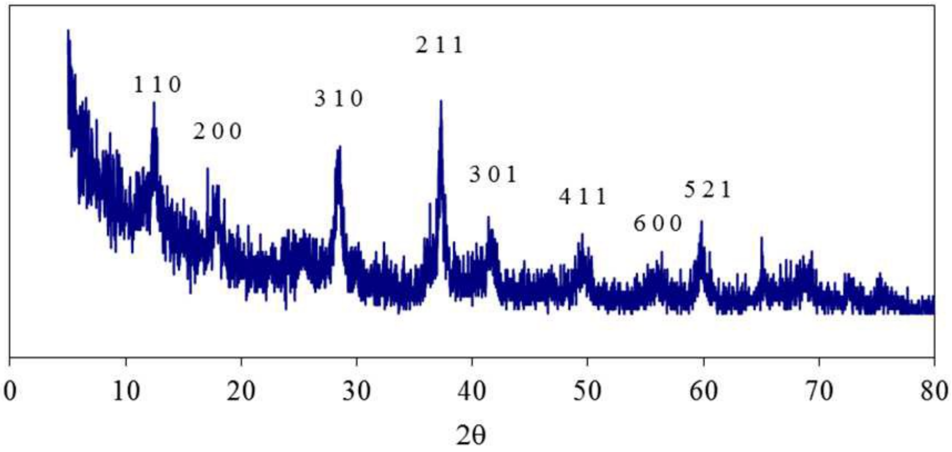

Fig. 2: XRD pattern of prepared MnO_2 nanocatalyst

Also, **Fig. 3** shows XRD patterns of the CuMn11, CuMn12, and CuMn13 mixed oxides catalysts. The pattern of CuMn11 exhibits new peaks compared to MnO_2 with high intensity (2θ = 30.89°, 35.7°) besides some characteristic peaks for CuO (2θ =

View Article Online
DOI: 10.1039/C7NJ04007E

35.77° and 48.5°) and MnO_2 ($2\theta = 28.03^o$, 41.49^o). These observations suggested the formation of new specific phase with spinel structure of copper-manganese is formed $CuMn_2O_4$ in CuMn11 sample due to the interaction between the two oxides during the co-precipitation at pH of 9 $CuMn_2O_4$ (ICDD-PDF no. 74–2422) [42]. The patterns of CuMn12 and CuMn13 have separated phases of crystalline MnO_2 and CuO. The intensity of the main peak of MnO_2 is enhanced, indicating the increase of the Mn concentration in the CuMn13 catalyst. Noticeably, the Mn_3O_4 phase was not detected in all samples.

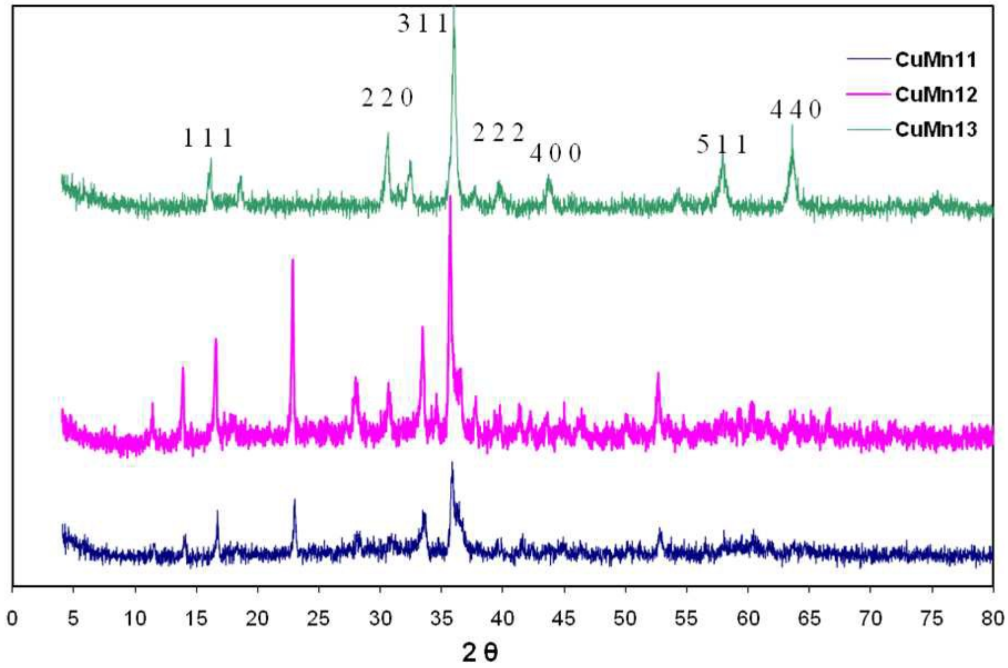

Fig. 3: XRD pattern of prepared Cu- Mn mixed oxides

3.1.2. Surface area analysis (BET)

Fig. 4 shows the corresponding N_2-adsorption-desorption isotherm, and pore size distributions. It is clear that the MnO_2 exhibits Type IV isotherm with the H1 hysteresis loop, which is a characteristic of open cylindrical pores. Pore size distribution driven by desorption branch confirms the MnO_2 nanorods possesses well-defined mesopore diameter. It should be noted that the hysteresis loop for MnO_2 is narrower due to the influence of mesopore interconnectivity on N_2 vaporization. The surface area of MnO_2

View Article Online
DOI: 10.1039/C7NJ04007E

was calculated to be 39.2 m^2/g using the BET method, and the total pore volume was 0.068 cm^3/g.

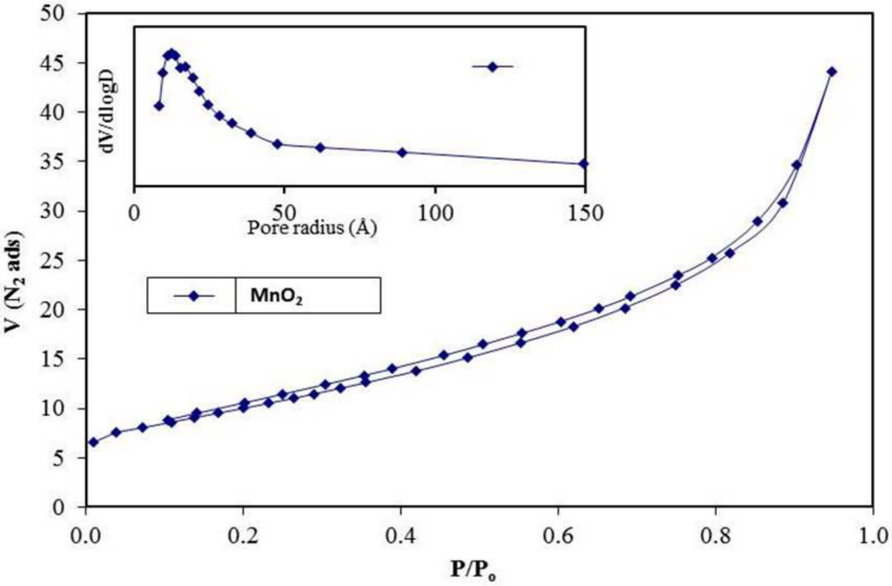

Fig. 4: (a) N_2- adsorption-desorption isotherm and (b) pore size distributions of MnO_2 nanocatalyst

The isotherms of CuMn11, CuMn12, and CuMn13 mixed oxide catalysts are typical of mesoporous solids according to IUPAC classification [43-45] with slow steepness adsorption of N_2 gas (**Fig. 5**). In all catalyst CuMn11, CuMn12 and CuMn13, the N_2-adsorption branch present an enhanced N_2-adsorption at P/P_0 in the regime of 0.8-0.98, which denotes the presence of an additional porosity. The absence of plateau is also giving an indication for the presence of voids between particles. The S_{BET} of CuMn11, CuMn12, and CuMn13 catalysts was 36, 30 and 22 m^2/g, respectively. The high surface of the CuMn11 catalyst may be due to the resultant spinal framework, which is in good agreement with XRD results. The pore size distribution corresponding to the CuMn11, CuMn12 and CuMn13 mesopores is centered around 3.77, 2.47 and 2.71 nm, respectively besides a relatively broad peak placed in the range of 3.8 nm, corresponding to the secondary porosity. The reduction in pore size accompanied with decreasing copper ratio may be due to the presence of copper in the outer surface of manganese pore. The pore volume of CuMn11, CuMn12, and CuMn13 was 0.067, 0.045 and 0.029 cm^3/g, respectively.

View Article Online
DOI: 10.1039/C7NJ04007E

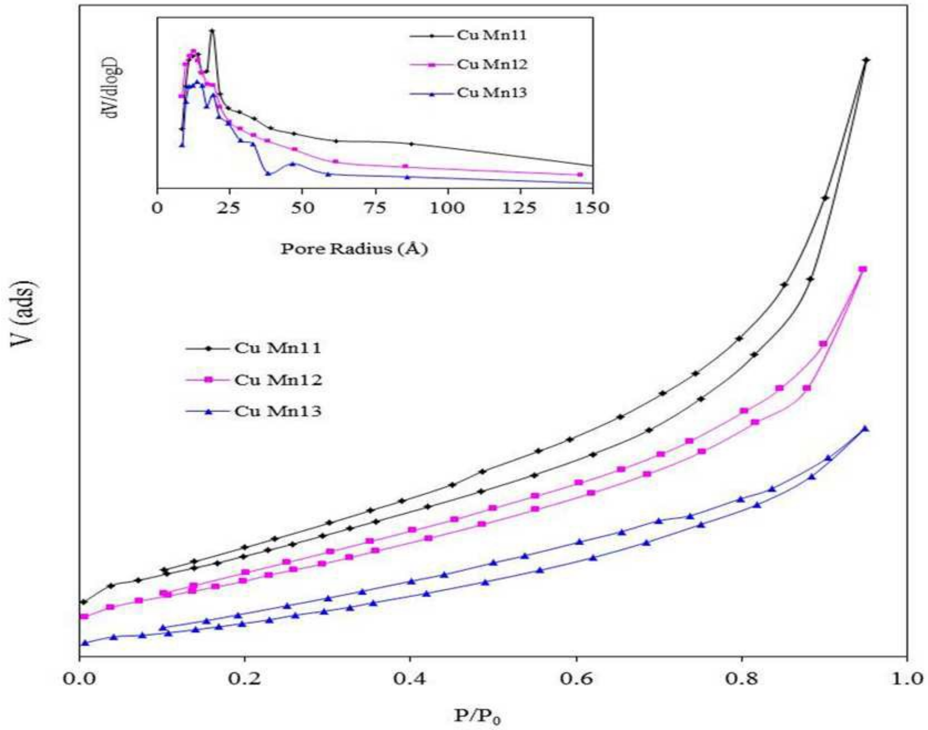

Fig. 5: (a) N_2- adsorption-desorption isotherm and (b) pore size distributions of Cu-Mn mixed oxide nanocatalysts

3.1.3. HRTEM of prepared nanocatalysts

HRTEM is a widely used technique in catalysis research field for collecting information about metal particle sizes and its morphology. The HRTEM analysis of nano MnO_2 catalyst is shown in **Fig. 6(a).** It reveals the formation of uniform rod-like morphology with different aspect ratios. The average dimensions calculated from the HRTEM micrographs ranged from ≈11 ± 3 nm widths and ≈ 58 ± 8 nm length. The high crystallinity of MnO_2 particles may result from ultrasonication effect during preparation. In case of CuMn11, HRTEM verifies the formation of the distorted oval shape with a particle size of 32 nm **Fig. 6(b) [26]**. Also, plate-like particles may be an ordered MnO_2 which intercalated through CuO particles and/or hydrogen bonding. When MnO_2 percent increased, these particles increased with enlargement. This clearly appears in **Fig. 5(c)** of CuMn12 catalyst photo also with the formation of small oval form with high extent of intramolecular spaces. Nevertheless, CuMn13 nanocatalyst appeared in parallel squared plates combined to each other. Their diameter is range between 28 - 40 nm as shown in **Fig. 6(d).** Agglomeration was clearly observed in **Fig.**

View Article Online
DOI: 10.1039/C7NJ04007E

6(b, c and d) due to hydrogen bonds between metal hydroxides and water molecules during calcinations that form bridges between adjacent particles [46, 47].

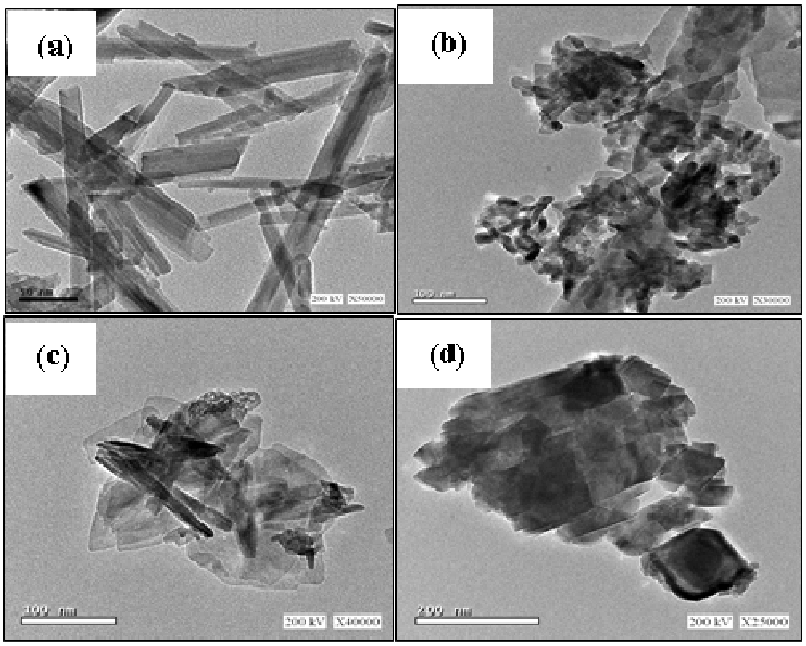

Fig. 6: HRTEM image of (a) MnO_2 nanorods, (b) CuMn11, (c) CuMn12 and (d) CuMn13

The X-ray photoelectron spectroscopy (XPS) of CuMn11 is shown in **Fig. 7a-c**. The XPS of Cu 2p core level exhibited peaks at 933.96 and 953.75 eV, which can be attributed to the BE (binding energy) of Cu $2p_{3/2}$ and Cu $2p_{1/2}$, indicating the presence of Cu^{2+} and Cu(I) species. Moreover, the ΔCu of split spin-orbit components is 19.79 eV, suggesting the presence of Cu–O species [43, 48]. In addition, the shake-up peak is observed at BE of 943.28 eV is due to an unfilled Cu_3d^9 shell, implying further indication for the presence of CuO species [43]. Two peaks can be observed at a binding energy (BE) about 642.1 and 653.8 eV, which are assigned to Mn $2p_{1/2}$ and Mn $2p_{3/2}$, respectively [49] (**Fig. 7b**). These peaks are curve-fitted into three peak components at BE of ~640.8, 641.7 and 642.9 eV, which assigned to Mn (II), Mn (III) and Mn (IV), respectively. The atomic ratio of Mn(II)/Mn(III) was of 1.1, reflecting the presence of Mn_3O_4 (MnO. Mn_2O_3). The CuMn11 exhibited a high ratio of Mn(III)/Mn(II) due to the presence of copper species inhibited the transformation of Mn(III) to Mn(II). The possible reason for the disappearance of Mn (IV) in XRD is that Mn_3O_4 composed of Mn (III) and Mn (II). The XPS of O 1s spectrum showed BE of 529.85, 531.37 and

View Article Online
DOI: 10.1039/C7NJ04007E

532.9 eV, corresponding to Mn–O–Mn, Mn–OH and crystalline water (H–O–H), respectively [50] (**Fig. 7c**). The Mn–OH species contribute about 12%, suggesting the CuMn11 offer high performance than Mn(II) due to the presence of hydroxyl group facilitate the redox property

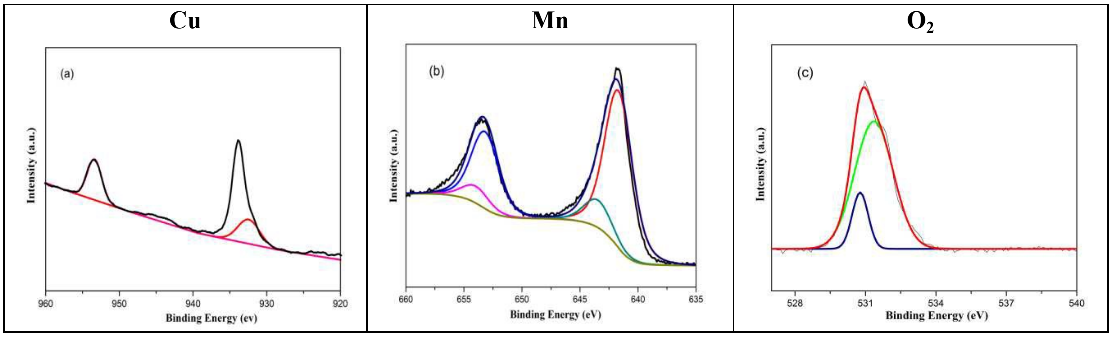

Fig. 7: The XPS spectra of CuMn11 nanocatalyst

3.2. The catalytic activity of prepared catalysts in TPA preparation

In this work, we evaluate the role of prepared MnO_2 nanorods and Cu-Mn mixed oxides as heterogeneous catalysts for the liquid phase oxidation of p-TA as a model reactant for highly pure TPA production **Scheme 3**. The reaction was also preceded via soluble metal acetates as homogenous ones by oxygen gas in the presence of NHSI (instead of Br_2) as a promoter. The synergetic effect of homogeneous and heterogeneous systems will be studied at different reaction time, catalyst weight, solvent types, pressures and reaction temperature for optimizing p-TA conversion (%) and TPA yield (%) according to the following scheme:

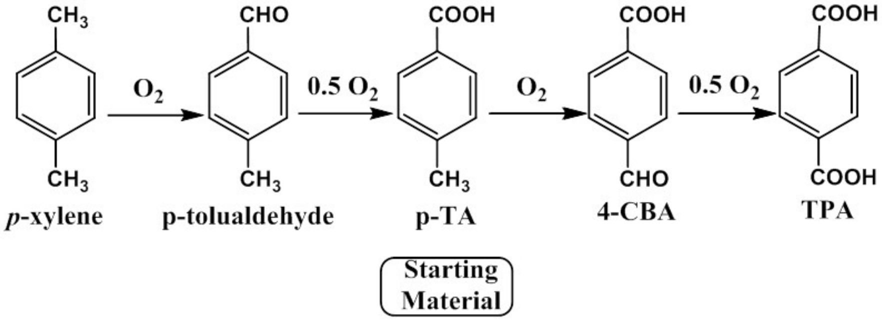

Scheme 3: Steps of PX oxidation with intermediates to form TPA

View Article Online
DOI: 10.1039/C7NJ04007E

3.2.1. Effect of reaction time

Many experiments were done to study the catalytic performance of a single metal oxide (MnO_2) and mixed metal oxides (Cu-Mn) for terephthalic acid production. The oxidation reaction is carried out at 1 atm oxygen pressure with the constant weight of catalyst (0.2 g) and NHSI by 1 h interval time up to 12 h in acetonitrile solvent.

Fig. 8 shows a diagram of TPA yield (%) against reaction time. It illustrates that all tested nanocatalysts donate low to a moderate yield of TPA ranged from ~ 16.8% to 46.6%. The most effective catalyst was CuMn11 while CuMn13 was the lowest one. CuMn11 initiated the oxidation reaction significantly after reaction time 2 h while MnO_2 and CuMn12 after 4 h, and the most delayed one was CuMn13, 6 h. The unique activity of CuMn11 relative to other catalysts may be due to its spinal structure which mostly has more oxygen vacancies promote the reaction [51-53]. Besides, the activity of MnO_2 and CuMn12 is more close to each other, this may be due to the formation of separated MnO_2 and CuO phases, and therefore MnO_2 component is mostly the effective part in CuMn12. These results coincided with HRTEM and XRD analysis (peak at $2\theta = 27.9^{\circ}$).

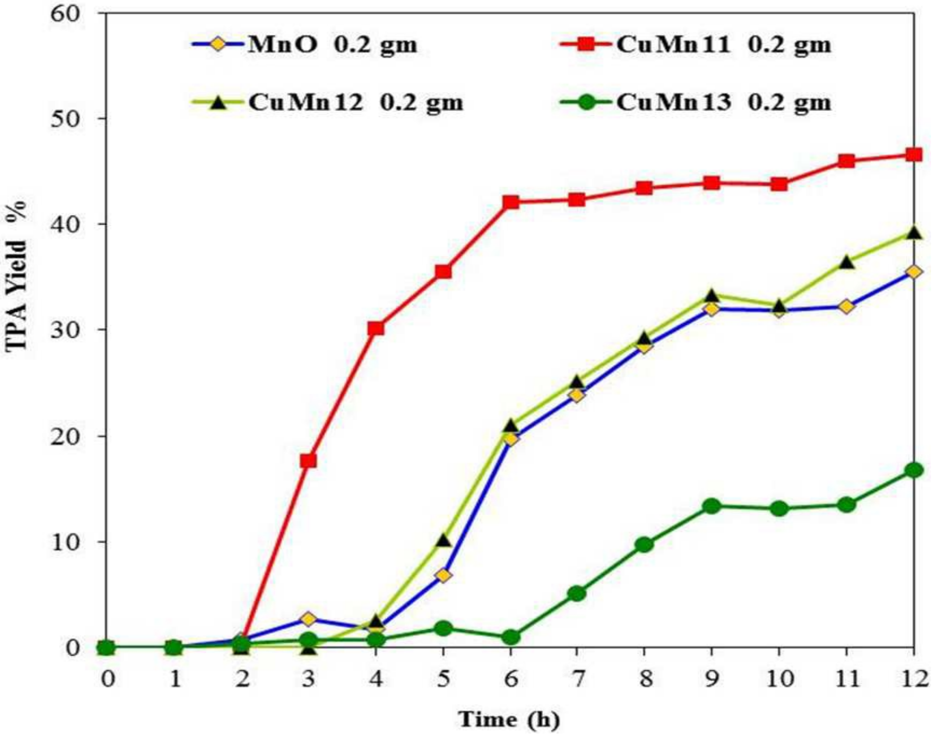

Fig 8: Effect of reaction time on TPA yield (%) using MnO_2 & Cu-Mn nanocatalysts

View Article Online
DOI: 10.1039/C7NJ04007E

Fig. 9 shows the yield of 4-CBA during 12 h by using MnO_2 and Cu-Mn nanocatalysts. It is clearly observed that formation of 4-CBA and TPA start at the same time after generating free radicals of NHSI for each catalyst. Lower initiation period is able to predict the expected higher catalyst performance. All tested catalysts resulted in fixed activity towards 4-CBA after 5 h of reaction time. After 12 h, MnO_2, CuMn11 and CuMn12 exhibit nearly the same results about 15% while CuMn13 tends to form lower yield (9.3%).

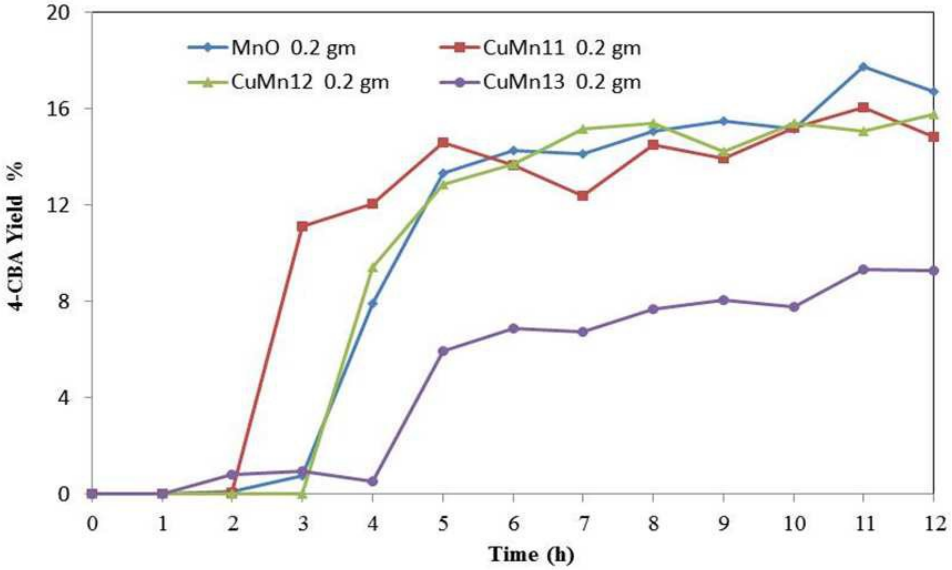

Fig 9: Effect of reaction time on 4-CBA yield (%) using MnO_2 and Cu-Mn nanocatalysts

3.2.2. Effect of catalyst weight

The oxidation reaction is carried out using different catalyst weights at 1 atm oxygen pressure in acetonitrile by 1 h interval time for 12 h. Catalyst weights were used 0.15, 0.20 and 0.40 g for the oxidation reaction. All results are collected in **Table 1**.

View Article Online
DOI: 10.1039/C7NJ04007E

Table 1: Oxidation of p-TA results with different catalysts and catalyst weights.

Catalyst	Weight (gm)	Conv. %	Yield %		Selectivity %	
		p-TA	TPA	4-CBA	TPA	4-CBA
MnO_2	**0.15**	36.4	19.8	16.6	54.5	45.5
	0.20	52.2	35.5	16.7	68.0	32.0
	0.40	52.6	34.1	18.4	64.9	35.1
CuMn 11	**0.15**	31.5	20.5	10.9	65.3	34.7
	0.20	62.4	47.6	14.8	76.3	23.7
	0.40	60.0	48.1	10.9	80.3	18.2
CuMn 12	**0.15**	24.1	14.3	9.8	59.5	40.5
	0.20	55.1	39.3	15.8	71.4	28.6
	0.40	40.5	28.8	11.8	71.0	29.0
CuMn 13	**0.15**	22.5	10.5	12.0	46.8	53.2
	0.20	26.1	16.8	9.3	64.4	35.6
	0.40	35.7	23.5	12.1	66.0	34.0

Reaction conditions: p-TA (80 mmol), NHSI (16 mmol) 0.4 mmol of each $Co(OAc)_2$ and $Mn(OAc)_2$ were dissolved in acetonitrile with bubbled pure oxygen gas and refluxed for 12 h at atm. pressure.

Table 1 displays the variation of catalyst weight effect on p-TA oxidation at the same abovementioned conditions. The catalyst weight effect correlated with p-TA conversion (%), TPA and 4-CBA yield and selectivity (%). It has been found that by increasing catalyst amount from 0.15 to 0.2 g, the conversion and yield (%) significantly increased especially with CuMn11 and CuMn12 which doubled, while excess weight to 0.4 g decreased the productivity except CuMn13. This may refer to that the obtained acidic products in reaction medium may be adsorbed and poised the catalyst active sites. On the other hand, CuMn13 sample has a higher concentration of secondary wider pores (~3.8 nm) which may facilitate adsorption of reactants and desorption of products on the catalyst surface, therefore, its catalytic activity increased by increasing the sample weight. The results of the yield and selectivity (%) are correlated together indicating that the optimum catalyst weight is 0.2 g of the best catalyst CuMn11, so no need for extra catalyst amount to improve the reaction outcomes.

3.2.3. Effect of solvent

The p-TA oxidation using prepared catalysts was carried out using different solvents like acetonitrile (polar), ethyl acetate (nonpolar), and a mixture of acetonitrile / acetic acid 9:1 (acidic). The last mixture was used to confirm the definite role of the acidic medium in target reaction.

View Article Online
DOI: 10.1039/C7NJ04007E

The results of different solvents are collected in **Table 2**. These experiments were carried out using optimum catalyst weight, 0.2 g, at 1 atm by refluxing for 12 h. It has been found that acetonitrile solvent achieved the best p-TA conversion (%), TPA and 4-CBA yield (%) and selectivity (%) values using all tested catalysts. Otherwise, the acidic solvent has the lowest rate. In acetonitrile, CuMn11 has great yield value (47.6%) rather than CuMn12 and MnO_2 which have a moderate yield (%) of TPA 39.3% and 35.5%, respectively. While the TPA yield (%) ranged from 11.1% to 18% by using ethyl acetate with all catalysts. This may occur due to the more solubility of oxygen gas in acetonitrile rather than ethyl acetate. Additionally, highly polar solvents like acetonitrile may facilitate the formation of active oxygen species and thereby enhance the catalytic activity [54]. Cu-Mn mixed oxides nanocatalysts exhibited nearly the same yield of terephthalic acid in an acidic solvent of 9.3% ± 0.5. Consequently, using this mixture as a solvent is excluded from our choices.

Table 2: Oxidation of p-TA results in different solvents with MnO_2 and Cu-Mn mixed oxides.

Catalyst	**Solvent**	**Conv. %**	**Yield %**		**Selectivity %**	
		p-TA	**TPA**	**4-CBA**	**TPA**	**4-CBA**
MnO_2	**ethyl acetate**	25.4	18.5	6.9	72.7	27.3
	acetonitrile	52.2	35.5	16.7	68.0	32.0
	ACN/ AcOH 9:1	9.5	4.5	5.0	47.2	52.8
CuMn 11	**ethyl acetate**	25.2	15.5	9.7	61.6	38.4
	acetonitrile	62.4	47.6	14.8	76.3	23.7
	ACN/ AcOH 9:1	27.2	10.5	16.7	38.7	61.3
CuMn 12	**ethyl acetate**	23.9	12.1	11.8	50.8	49.2
	acetonitrile	55.1	39.3	15.8	71.4	28.6
	ACN/ AcOH 9:1	18.1	9.3	8.8	51.6	48.4
CuMn 13	**ethyl acetate**	20.4	11.1	9.3	54.5	45.5
	acetonitrile	26.1	16.8	9.3	64.4	35.6
	ACN/ AcOH 9:1	21.7	8.8	12.8	40.7	59.3

Reaction conditions: p-TA (80 mmol), NHSI (16 mmol), 0.2 gm catalyst and 0.4 mmol of each $Co(OAc)_2$ and $Mn(OAc)_2$ were dissolved in selected solvent with bubbled pure oxygen gas and refluxed for 12 h at 1 atm..

3.2.4. Effect of oxygen pressure

One of the most vital parameter which is closely related to industrial processes is the oxygen gas pressure [55]. Therefore, the oxidation of p-TA was studied extensively at different pressures, 10, 15 and 20 atm, by using the most efficient solvents acetonitrile and ethyl acetate with different temperatures (110 and 150 °C) for reaction time 12 h and the other conditions remained the same. The values of p-TA conversion (%), TPA yield (%) and selectivity (%) related to pressure and temperature are shown in **Table 3.**

View Article Online
DOI: 10.1039/C7NJ04007E

Table 3: Oxidation of p-TA with MnO_2 and Cu-Mn nanocatalysts in different oxygen pressure, reaction temperature and solvents.

Catalyst	Pressure (atm)	Temperature (°C)	Solvent	Conv. %	Yield %	Selectivity %
				p-TA	TPA	TPA
MnO_2	10	110	acetonitrile	74.6	64.0	85.8
	15	110	acetonitrile	78.6	66.0	84.0
	20	110	acetonitrile	76.4	70.5	92.3
	20	150	acetonitrile	86.7	75.8	87.4
	20	110	ethyl acetate	88.6	70.4	79.5
	20	150	ethyl acetate	**90.1**	88.9	**98.7**
CuMn 11	10	110	acetonitrile	82.0	69.9	85.2
	15	110	acetonitrile	85.0	73.9	86.9
	20	110	acetonitrile	84.6	79.6	94.1
	20	150	acetonitrile	**99.5**	**99.1**	**99.6**
	20	110	ethyl acetate	**99.1**	**97.0**	**97.9**
	20	150	ethyl acetate	**99.6**	**97.6**	**98.0**
CuMn 12	10	110	acetonitrile	81.7	68.9	84.3
	15	110	acetonitrile	82.2	69.5	84.5
	20	110	acetonitrile	84.4	72.5	85.9
	20	150	acetonitrile	81.8	74.7	91.3
	20	110	ethyl acetate	**97.0**	**96.0**	**99.0**
	20	150	ethyl acetate	**96.2**	**94.7**	**98.4**
CuMn 13	10	110	acetonitrile	87.5	79.8	91.2
	15	110	acetonitrile	88.0	81.1	92.2
	20	110	acetonitrile	**96.5**	87.8	91.0
	20	150	acetonitrile	**97.3**	**93.3**	**95.9**
	20	110	ethyl acetate	**97.9**	**94.7**	**96.7**
	20	150	ethyl acetate	**98.3**	**95.1**	**96.7**

Reaction conditions: p-TA (80 mmol), NHSI (16 mmol), 0.2 gm catalyst and 0.4 mmol of each $Co(OAc)_2$ and $Mn(OAc)_2$ were dissolved in a selected solvent with different pure oxygen pressures for 12 h.

It describes that TPA yield (%) increases gradually with increasing the oxygen pressure at 110 °C using all catalysts in acetonitrile. The conversion and yield (%) values reach to 96.5 and 87.8 %, respectively, and the selectivity towards TPA was major with CuMn11 at 110 °C, however, when reaction temperature raised to 150 °C, these values were greatly improved especially in case of CuMn11 and MnO_2. The best oxidation activity was achieved with CuMn11 in acetonitrile at 20 atm and 150 °C as p-TA conversion (%) and TPA selectivity (%) 95.5 and 99.6 respectively.

By using ethyl acetate solvent, all tested catalysts achieved magnificent conversion and yield percents at both 110 °C and 150 °C. Generally, CuMn11 was the most efficient oxidation catalyst at different conditions. Also, CuMn12 achieved great

DOI: 10.1039/C7NJ04007E

improvement of conversion; yield and selectivity percents at 110 °C besides CuMn13 and MnO_2 have distinguished results of conversion and yield at 150 °C.

Water molecules which are produced as a by-product of equimolar amounts in oxidation with molecular oxygen can be strongly adsorbed on metals oxide surfaces via hydrogen bonding which block catalysts active sites [56]. So, the polarity of solvent is recommended when the reaction was preceded at a temperature lower than 100°C but, at > 100 °C, water molecules could be in the vapor phase with each solvent keeping free active sites on catalyst surface dry [32, 57]**.** The prominent effect of pressure may be due to using closed system high-pressure reactor which allowed raising the reaction temperature more than the boiling point of the selected solvent (≥88°C). Ethyl acetate as a nonpolar solvent could obtain good catalytic oxidation activity.

It is concluded that homogeneous catalytic system is mostly helpful in p-TA oxidation at 1 atm. Previous experiments at high pressure were also carried out using the dual catalytic systems. Now, it is claimed to assign the role of prepared mixed metal oxide, using the most efficient catalyst sample (CuMn11) without utilizing homogenous catalyst (cobalt (II) acetate and manganese (II) acetate) at 20 atm and 150 °C for 12 h in acetonitrile solvent. As shown in Table 4, CuMn11 achieved the same conversion (%) of p-TA with a slight decrease in the yield of TPA by 1.4% only without homogeneous systems in presence or absence of a homogeneous catalyst. Under the same conditions, the reaction which proceeds without solid metal oxide in the presence of homogeneous catalyst showed the conversion of p-TA, and TPA yield (%) decreased to 65%, and 54.1%, respectively. These results confirm the integrated activity of CuMn11 for catalytic oxidation of p-TA, and there is no need for the homogeneous catalysis for the oxidation reaction as shown in **Table 4**.

View Article Online
DOI: 10.1039/C7NJ04007E

Table 4: the role of CuMn11 for oxidation of p-toluic acid without homogenous catalysts at optimum conditions.

Catalyst	Metal Acetates	Pressure (atm)	Temperature (°C)	Solvent	Conv. %	Yield %	Selectivity %
					p-TA	TPA	TPA
CuMn 11	+	20	150	acetonitrile	99.5	99.1	99.6
	-	20	150	acetonitrile	99.5	97.7	98.1
CuMn 11	+	20*	150	acetonitrile	≈0	0	0
Without catalyst	+	20	150	acetonitrile	65.4	54.1	82.7

The symbols + and – means the reaction is carried out in the presence or absence of the homogeneous catalyst
* means the reaction is carried out using N_2 gas

4. The proposed reaction mechanism

As shown in **Scheme 4**, the catalysis occurs by a free radical mechanism. The oxidation reaction is initiated by generation of the succinimide-N-oxyl radical (SINO) by abstraction of the (O-H) hydrogen in NHSI. Through homogenous metal ions, SINO is created by highly active M^{3+}-dioxygen radical that formed by molecular oxygen in addition to, mixed metal oxide surface with lattice oxygen and oxygen vacancies may contribute in the formation of SINO radical by further two pathways. First, (M=O) and adsorbed oxygen could abstract hydrogen of NHSI forming hydroxyl and hydroperoxyl radicals. Second, these radicals could pick up other hydrogen atoms giving away water molecules. It should be noted that active sites on mixed metal oxide are regenerated by molecular oxygen. The SINO radicals then abstract a hydrogen atom from methyl group of target p-TA, thus reverting NHSI and a carbon-centered radical. This carbon radical reacts with O_2 to yield an alkylperoxy radical which subsequently abstracts the (O-H) hydrogen from NHSI, forming a stable hydroperoxide. Then, hydroperoxide is dissociated by metal ions and complete oxidation by oxygen to form carboxyl group. The formation of excess SINO radicals by using metal oxide explains clearly the role of mixed metal oxide with NHSI via oxidation reaction of p-TA.

View Article Online
DOI: 10.1039/C7NJ04007E

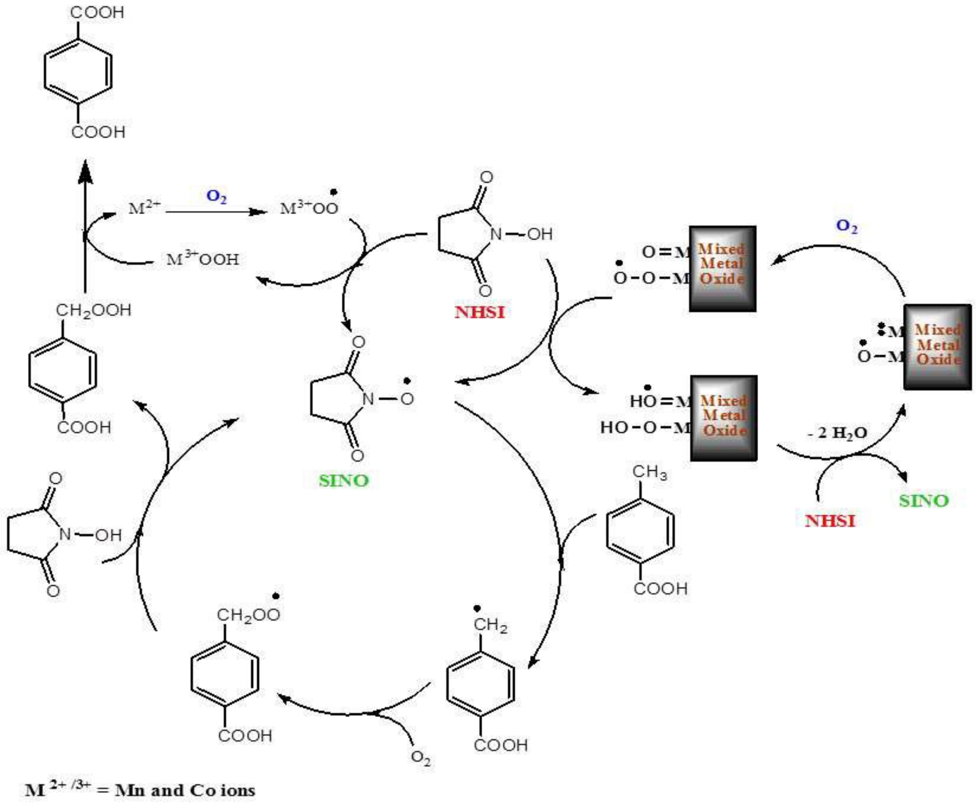

Scheme 4: Mechanism of p-TA oxidation reaction by O_2 with NHSI/ mixed metal oxide.

5. Conclusion

The catalytic activity of MnO_2 nano-rods comparing with Cu-Mn mixed oxides nanoparticles has been entirely examined for the oxidation of p-TA to produce TPA. Cu-Mn mixed oxides nanoparticles achieved great activity at 20 atm in both acetonitrile and ethyl acetate solvents rather than single metal oxide MnO_2 with and without homogeneous. The superior catalytic activity achieved with CuMn11 nanocatalyst at 20 atm oxygen pressure due to the high distribution of both Mn^{3+}, Mn^{4+} ions, and $Cu^{+,}$ Cu^{2+} ions in spinel structure containing as formed two Jahn–Teller ions (Cu^{2+} and Mn^{3+}) that enable the redox cycle of the two metals with distinctive surface properties as very high conversion 99.5% and yield 99.1% in acetonitrile at 150°C. Deeply, this system suppressed the presence of 4-CBA intermediate (impurity) by using NHSI (instead of Br_2) as a promoter in a solvent rather than acetic acid. Therefore, the presence of copper oxide combined with manganese oxide appends great influence on catalytic activity towards TPA formation. Furthermore, it shows the effect of mixing two different metal

DOI: 10.1039/C7NJ04007E

ions with various oxidation states and their role in the excessive formation of free radicals that push the rate of reaction.

conflict of interest

There are no conflicts of interest to declare

DOI: 10.1039/C7NJ04007E

References

1. S. S. Acharyya, S. Ghosh, S. Adak, R. Singh, S. Saran and R. Bal, *Journal of Nanoscience and Nanotechnology*, 2015, **15**, 5816-5822.
2. S. S. Acharyya, S. Ghosh and R. Bal, *Green Chem.*, 2015, **17**, 3490-3499.
3. S. Ishikawa and W. Ueda, *Catalysis Science & Technology*, 2016, **6**, 617-629.
4. M. A. Betiha, A. M. Rabie, H. S. Ahmed, A. A. Abdelrahman and M. F. El-Shahat, *Egyptian Journal of Petroleum*, 2017.
5. P. L. Mills and R. V. Chaudhari, *Catalysis Today*, 1999, **48**, 17-29.
6. W. Partenheimer, *Applied Catalysis A: General*, 2011, **409**, 48-54.
7. K. Deori, D. Gupta, B. Saha, S. K. Awasthi and S. Deka, *Journal of Materials Chemistry A*, 2013, **1**, 7091-7099.
8. S. Sakaguchi, T. Hirabayashi and Y. Ishii, *Chemical Communications*, 2002, 516-517.
9. Y. Ishii, S. Sakaguchi and Y. Obora, in *Modern Oxidation Methods*, Wiley-VCH, 2005, DOI: 10.1002/9783527632039.ch6, pp. 187-240.
10. N. Hirai, Y. Tatsukawa, M. Kameda, S. Sakaguchi and Y. Ishii, *Tetrahedron*, 2006, **62**, 6695-6699.
11. Y. Aoki, S. Sakaguchi and Y. Ishii, *Tetrahedron*, 2006, **62**, 2497-2500.
12. E. L. Clennan, *Singlet Oxygen: Applications in Biosciences and Nanosciences Volume 1*, 2016, 353.
13. Y. Aoki, N. Hirai, S. Sakaguchi and Y. Ishii, *Tetrahedron*, 2005, **61**, 10995-10999.
14. Y. Ishii and S. Sakaguchi, *Catalysis Today*, 2006, **117**, 105-113.
15. K. Kamae, Y. Obora and Y. Ishii, *Bulletin of the Chemical Society of Japan*, 2009, **82**, 891-895.
16. F. Minisci, F. Recupero, G. F. Pedulli and M. Lucarini, *Journal of Molecular Catalysis A: Chemical*, 2003, **204**, 63-90.
17. D. Habibi, A. R. Faraji, M. Arshadi, S. Heydari and A. Gil, *Applied Catalysis A: General*, 2013, **466**, 282-292.
18. L. Melone, S. Prosperini, G. Ercole, N. Pastori and C. Punta, *Journal of Chemical Technology and Biotechnology*, 2014, **89**, 1370-1378.
19. L. Melone and C. Punta, in *Liquid Phase Aerobic Oxidation Catalysis: Industrial Applications and Academic Perspectives*, 2016, DOI: 10.1002/9783527690121.ch16, pp. 253-265.
20. C. Miao, H. Zhao, Q. Zhao, C. Xia and W. Sun, *Catalysis Science & Technology*, 2016, **6**, 1378-1383.
21. Y. Tashiro, T. Iwahama, S. Sakaguchi and Y. Ishii, *Advanced Synthesis & Catalysis*, 2001, **343**, 220-225.
22. S. S. Stahl and P. L. Alsters, *Liquid Phase Aerobic Oxidation Catalysis: Industrial Applications and Academic Perspectives*, John Wiley & Sons, 2016.
23. W. Partenheimer, *Advanced Synthesis & Catalysis*, 2004, **346**, 1495-1500.
24. W. Partenheimer, *Journal of Molecular Catalysis A: Chemical*, 2003, **206**, 105-119.
25. Y. Tashiro, T. Iwahama, S. Sakaguchi and Y. Ishii, *Advanced Synthesis & Catalysis*, 2001, **343**, 220-225.
26. Y. Ishii and S. Sakaguchi, *Catalysis Today*, 2006, **117**, 105-113.
27. J. F. Gomes, *Chemical Reviews*, 2013.
28. L. Melone and C. Punta, *Beilstein Journal of Organic Chemistry*, 2013, **9**, 1296-1310.
29. I. E. Wachs and K. Routray, *ACS Catalysis*, 2012, **2**, 1235-1246.
30. S. Nicolae, F. Neaţu and M. Florea, *Comptes Rendus Chimie*, 2017, **in press**, 1-8.

View Article Online
DOI: 10.1039/C7NJ04007E

31. R. r. A. Tomás, J. o. C. Bordado and J. o. F. Gomes, *Chemical reviews*, 2013, **113**, 7421-7469.
32. N. A. M. Fadzil, M. H. A. Rahim and G. P. Maniam, *Chinese Journal of Catalysis*, 2014, **35**, 1641-1652.
33. D. S. Kim, Y. H. Shin and Y.-W. Lee, *Chemical Engineering Communications*, 2015, **202**, 78-84.
34. J. M. Tibbitt, W. H. Gong, W. P. Schammel, R. P. Hepfer, V. Adamian, S. P. Brugge, P. D. Metelski and C. Zhou, *Journal*, 2007.
35. S. Chavan, D. Srinivas and P. Ratnasamy, *Journal of Catalysis*, 2001, **204**, 409-419.
36. Q. Wang, X. Li, L. Wang, Y. Cheng and G. Xie, *Industrial & engineering chemistry research*, 2005, **44**, 261-266.
37. J. W. Kwak, J. S. Lee and K. H. Lee, *Applied Catalysis A: General*, 2009, **358**, 54-58.
38. N. Taha, M. Chidambaram, J. Dakka and Y. Sasson, *Catalysis letters*, 2009, **129**, 358-362.
39. A. Shaabani and A. Rahmati, *Catalysis Communications*, 2008, **9**, 1692-1697.
40. R. Kannan, A. Jegan, A. Ramasubbu, K. Karunakaran and S. Vasanthkumar, *Dig J Nanomat Biostruct*, 2011, **6**, 755-760.
41. C.-C. Kuo, W.-J. Lan and C.-H. Chen, *Nanoscale*, 2014, **6**, 334-341.
42. P. Ma, Q. Geng, X. Gao, S. Yang and G. Liu, *Ceramics international*, 2016, **42**, 11966-11973.
43. A. M. Rabie, M. A. Betiha and S.-E. Park, *Applied Catalysis B: Environmental*, 2017.
44. S. K. Mohamed, A. A. Ibrahim, A. Mosa, M. A. Betiha, E. El-Sharkawy and H. M. Hassan, *Separation and Purification Technology*, 2017.
45. M. Betiha, A. Rabie, A. Elfadly and F. Yehia, *Microporous and Mesoporous Materials*, 2016, **222**, 44-54.
46. B. Faure, G. Salazar-Alvarez, A. Ahniyaz, I. Villaluenga, G. Berriozabal, Y. R. De Miguel and L. Bergström, *Science and technology of advanced materials*, 2013, **14**, 023001.
47. F. Fu, Z. Cheng and J. Lu, *RSC Adv.*, 2015, **5**, 85395-85409.
48. D.-W. Kim, K.-Y. Rhee and S.-J. Park, *Journal of Alloys and Compounds*, 2012, **530**, 6-10.
49. B. Puértolas, A. Smith, I. Vázquez, A. Dejoz, A. Moragues, T. Garcia and B. Solsona, *Chemical engineering journal*, 2013, **229**, 547-558.
50. T.-H. Wu, D. Hesp, V. Dhanak, C. Collins, F. Braga, L. J. Hardwick and C.-C. Hu, *Journal of Materials Chemistry A*, 2015, **3**, 12786-12795.
51. X. Shi, S. L. Bernasek and A. Selloni, *The Journal of Physical Chemistry C*, 2016, **120**, 14892-14898.
52. S. Dey, G. C. Dhal, R. Prasad and D. Mohan, *Bulletin of Chemical Reaction Engineering & Catalysis*, 2017.
53. X. Wang, Z. Lan, Y. Liu, Y. Luo, J. Chen, L. Jiang and Y. Wang, *Chemical Communications*, 2017, **53**, 967-970.
54. V. MAHDAVI and M. MARDANI, *Journal of Chemical Sciences*, 2012, **124**, 1107-1115.
55. S. Matar, M. J. Mirbach and H. A. Tayim, in *Catalysis in Petrochemical Processes*, Springer Netherlands, Dordrecht, 1989, DOI: 10.1007/978-94-009-1177-2_5, pp. 84-108.
56. C. Keresszegi, J. D. Grunwaldt, T. Mallat and A. Baiker, *Journal of Catalysis*, 2004, **222**, 268-280.
57. G. Yang, L. Wang, J. Li, Y. Zhang, X. Dong, Y. Lv and S. Gao, *Research on Chemical Intermediates*, 2012, **38**, 775-783.

Challenges and technological opportunities of nano-mixed oxide (Cu–Mn) allow green route to valued terephthalic acid production from p-xylene.